minerals

MDPI

Article

Re-Os Geochronology, Whole-Rock and Radiogenic Isotope Geochemistry of the Wulandele Porphyry Molybdenum Deposit in Inner Mongolia, China, and Their Geological Significance

Xiaojun Zhang [1,2,*], Chunliang Yao [1,2,*], David R. Lentz [3], Ying Qin [1], Yiwen Wei [1], Fengshun Zhao [1], Zhen Yang [1,2], Rui Liu [1,2] and Zhenfei Zhang [1]

1 School of Earth Resources, China University of Geosciences, Wuhan 430074, China
2 National Demonstration Center for Experimental Mineral Exploration Education, China University of Geosciences, Wuhan 430074, China
3 Department of Earth Sciences, University of New Brunswick, Fredericton, NB E3B5A3, Canada
* Correspondence: xjzhang01@cug.edu.cn (X.Z.); yaochunliang@189.cn (C.Y.)

Received: 24 March 2020; Accepted: 15 April 2020; Published: 21 April 2020

Abstract: The Wulandele molybdenum deposit is a porphyry-type Mo deposit in the Dalaimiao area of northern Inner Mongolia, China. Molybdenite Re-Os dating yields a model age of 134.8 ± 1.9 Ma, with the fine-grained monzogranite most closely related to the mineralization. The lithogeochemical data show that the monzogranite is weakly peraluminous, high-K calc-alkaline series, with reduced to slightly oxidized, highly fractionated I-type granite characteristics. The relatively low initial $^{87}Sr/^{86}Sr$ (range from 0.705347 to 0.705771), weakly negative $\varepsilon_{Nd}(t)$ (range from −2.0 to −1.3), and crust-mantle mixing of Pb isotopes suggest that the monzogranite originated from the partial melting of mafic juvenile lower continental crust derived from the depleted mantle, with a minor component of ancient continental crust. Combined with the regional tectonic evolution, we argue that the partial melting, then injection, of the monzogranite melt was probably triggered by collapse or delamination of the thickened lithosphere, which was mainly in response to the post-orogenic extensional setting of the Mongol–Okhotsk belt; this is possibly coupled with a back-arc extension related to Paleo-Pacific plate subduction. The extensively fractional crystallization of the monzogranite melt is the crucial enrichment process, resulting in magmatic hydrothermal Mo mineralization in the Wulandele deposit, and the Cretaceous granitoids are generally favorable to form Mo mineralization in the Dalaimiao area.

Keywords: Re-Os geochronology; geochemistry; Sr-Nb-Pb isotopes; Wulandele porphyry molybdenum deposit; Inner Mongolia

1. Introduction

In the past two decades, several molybdenum deposits, such as the Wulandele, Wurnitu, Zhunsujihua, Wuhua'aobao, and Dalaiaobao molybdenum deposits, have been found in the Dalaimiao area, which is located in the southwest of Xing'an-Mongolia Orogenic Belt (XMOB) [1–6] (Figure 1). These molybdenum deposits have close temporal-spatial relationships with intermediate-felsic intrusive rocks, and most of them formed in late Jurassic to early Cretaceous, except the Zhunsujihua Mo deposit, which formed during the late Carboniferous to early Permian [1–6]. Among these molybdenum deposits, the Wulandele is a porphyry-type deposit formed during the Mesozoic in the Erlian-Dongwuqi metallogenic belt, which was discovered in 2006 by the Inner Mongolia Institute Geological Survey [1,7]. The molybdenite in the Wulandele Mo deposit mainly occurs within the inner contact zone of the fine-grained monzogranite (MG) and its wall rocks, with minor development as veins in the wall rocks,

which are composed of the main Permian quartz diorite (QD) and, locally, granodiorite (GD) [1,7]. There is some research on the geological features, ore-related intrusions, ore-forming fluid, and Mo mineralization age of this deposit [1,7,8]. Tao et al. [1,7] reported a molybdenite Re-Os isochron age of 134.1 ± 3.3 Ma and zircon SHRIMP U-Pb dating of 131.3 ± 1.6 Ma for the MG, and suggested that Mo mineralization has a genetic relationship with the MG. However, detailed petrology, geochemical, and isotopic data have not been investigated for the MG, which is important to interpret its magmatic source and evolution, tectonic setting, and mineralized significance.

In this contribution, detailed research on the petrology, geochemistry, and radiogenic (Sr-Nb-Pb) tracer isotopes for the MG have been carried out to improve our understanding of the genesis and the geodynamic setting of the fine-grained monzogranite and the associated Mo mineralization. Furthermore, this research analyzed the redox conditions, assimilation, and extensive fractional crystallization processes of the MG to evaluate the controlling factors of Mo mineralization.

2. Geological Background and Petrological Characteristics

The Dalaimiao area, located in the southwestern Xing'an Block in northeast China (Figure 1), has already become recognized as a new Mo-mineralized area that has experienced increased exploration this last decade [5,6]. The Xing'an Block is one section of XMOB, which is regarded as the southeast part of the Central Asian Orogenic Belt (CAOB), and can be subdivided into four blocks (the Erguna, Xing'an, Songliao, and Jiamusi blocks) from northwest to southeast by the Xiguitu–Tayuan, Hengenshan–Heihe, and Jiayin–Mudanjiang faults [9,10].

The Xing'an Block (XB) is characterized by widespread late Paleozoic and Mesozoic granitoid, Jurassic–Early Cretaceous volcanic rocks, and a paucity of deformed and metamorphosed pre-Mesozoic terrains [10]. The NE- and ENE-trending faults controlled the distribution of the stratigraphy and magmatic rocks. Wu et al. [11] identified four stages of granitic magmatism in the XB: (1) Carboniferous I-type granitoids (340 to 300 Ma), which are rarely developed in the terrane, comprising gabbro, diorite, granodiorite, and monzogranite; (2) Permian A-type granitoids (290 to 260 Ma), which occur as part of a huge Late Paleozoic A-type granitic belt that extends from Xinjiang through southern Mongolia to central Inner Mongolia; (3) Middle Jurassic granitoids (187 to 157 Ma); (4) Early Cretaceous granites (145 to 106 Ma), which represent the most important stage of granitic magmatism in this block, extending in an NNE direction and crossing the block boundaries.

The Wulandele Mo deposit is located in the Baiyinwula–Sonidzuoqi area of Inner Mongolia, which is situated near the border of China and Mongolia at geographic coordinates of E 112°50′00″ to E 112°52′00″ and N 44°48′30″ to N 44°49′15″; it belongs to the Dongwuqi–Erenhot polymetallic metallogenic belt. A large number of intrusive rocks with several small felsic dykes and quartz veins are exposed on surface at the Wulandele deposit, and small amounts of Quaternary gravel, sand, and clay are distributed locally in the exploration area. The intrusive rocks include the Carboniferous biotite granite (BG), the Permian quartz diorite (QD, locally occurring as granodiorite in the deep, GD), and the concealed MG. The QD is exposed in the middle of the mine area as a stock of 3 km^2 and intruded into the BG, which is part of the regional granitic batholith (Figure 2). The concealed MG stock discovered in drill cores intruded into the QD and GD. The NW-trending fractures, which are the major ore-bearing faults of the Mo deposit, are extremely abundant in the mine area and are commonly controlling structures for felsic dykes and ore-bearing quartz veins (Figure 2). Although less obvious, the NE-trending faults are present outside the mine area, with a trend consistent with the predominant regional faults.

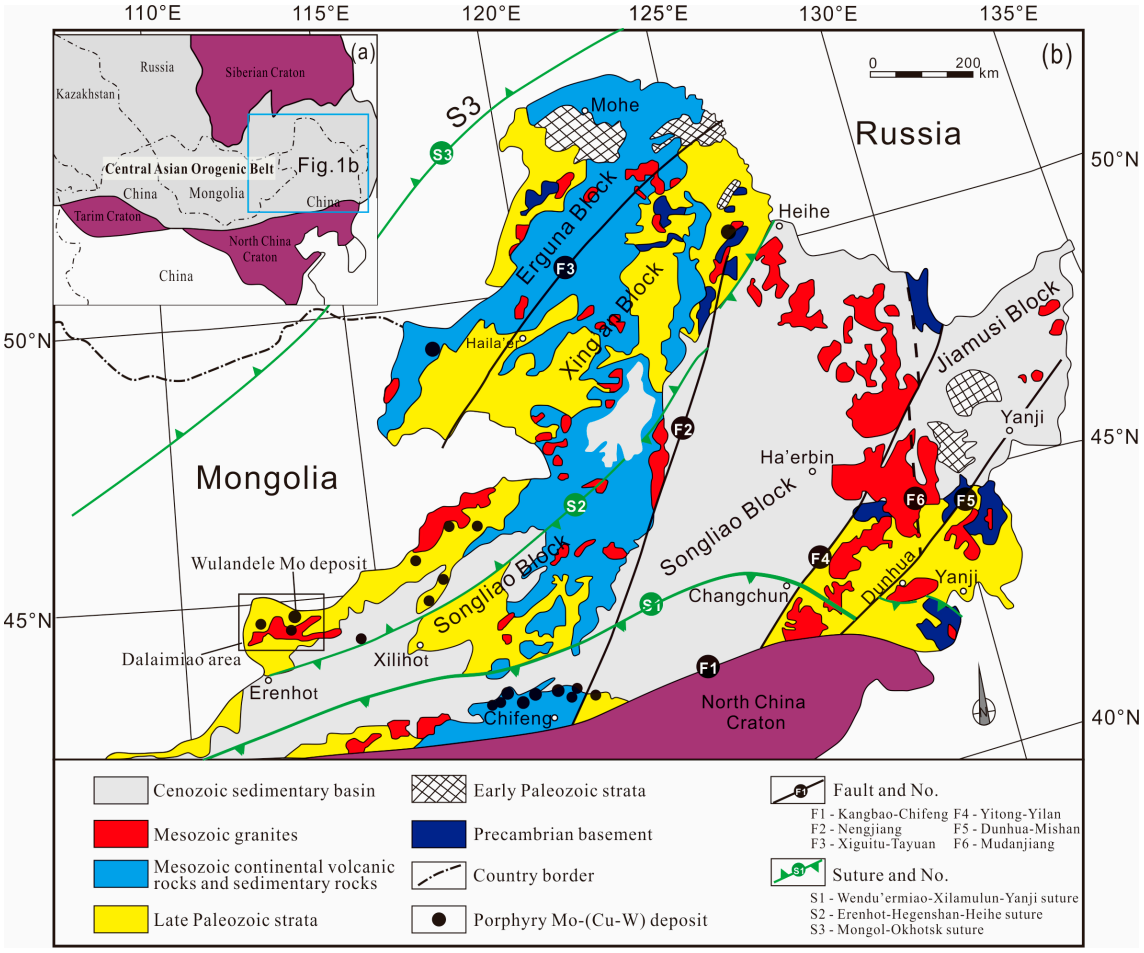

Figure 1. Regional tectonic map of the Xing'an–Mongolia Orogenic Belt in Inner Mongolia (**a** after [10,12,13]). The insert is a simplified map showing the position of Xing'an–Mongolia Orogenic Belt in the eastern Central Asian Orogenic Belt (**b** after [14]).

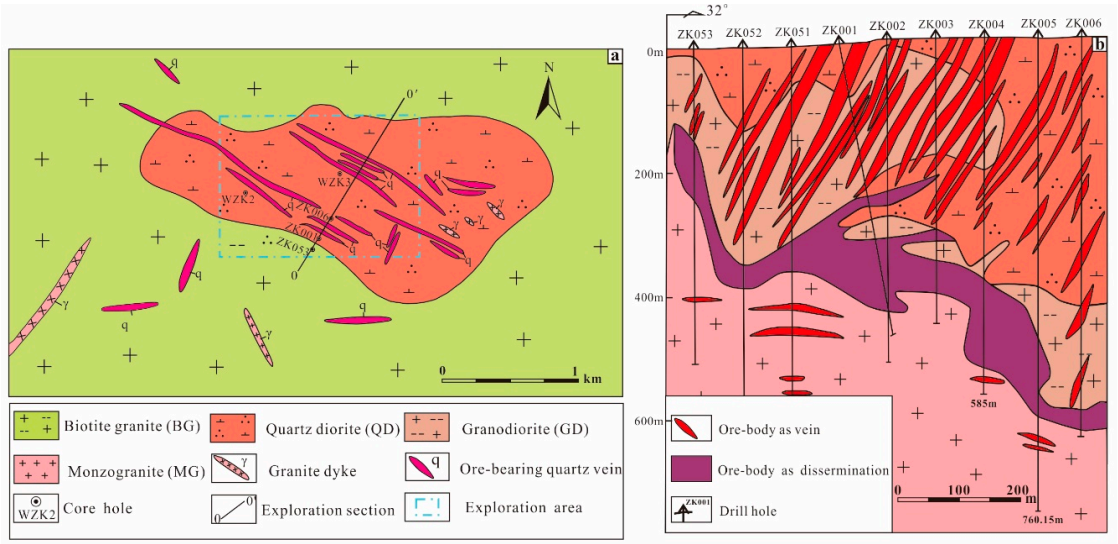

Figure 2. Geological sketch map (**a**) and exploration Section 0–0′ (**b**) of the Wulandele molybdenum deposit (after [1]).

The BG is gray-red-coloured, medium- to coarse-grained, seriate-textured, and consists of alkali feldspar (35–40%), plagioclase (25–30%), quartz (25–30%), and biotite (5–10%), with minor accessory minerals (1–2%). The QD is dark grayish, has fine- to medium-grained granitic texture (Figure 3a–c) and consists of plagioclase (40–55%), quartz (10–15%), alkali feldspar (5–10%), biotite (15–25%), and hornblende (1–4%), with minor accessory minerals (1–2%). The GD is grayish, with fine- to medium-grained granitic texture (Figure 3d–f) and consists of plagioclase (45–55%), alkali feldspar (18–20%), quartz (20–25%), biotite (10–15%), and hornblende (1–4%) with minor accessory minerals (1–2%). The QD has a zircon U-Pb age of 292.6 ± 0.5 Ma reported by Tao et al. [1]. The MG is pink-coloured, with fine-grained granitic texture (Figure 3a,b,g,h), and consists of quartz (30–35%), alkali feldspar (30–35%), plagioclase (25–30%), and biotite (1–3%), with minor accessory minerals, such as ilmenite, zircon, and monazite (1–2%). The MG has a zircon U-Pb age of 131.3 ± 1.6 Ma [7] and was pervasively overprinted by potassic and quartz–sericite alteration, with obviously disseminated Mo mineralization at its roof. The MG was regarded as the ore-related granite based on the geologic and geochronologic evidence [1,7,8].

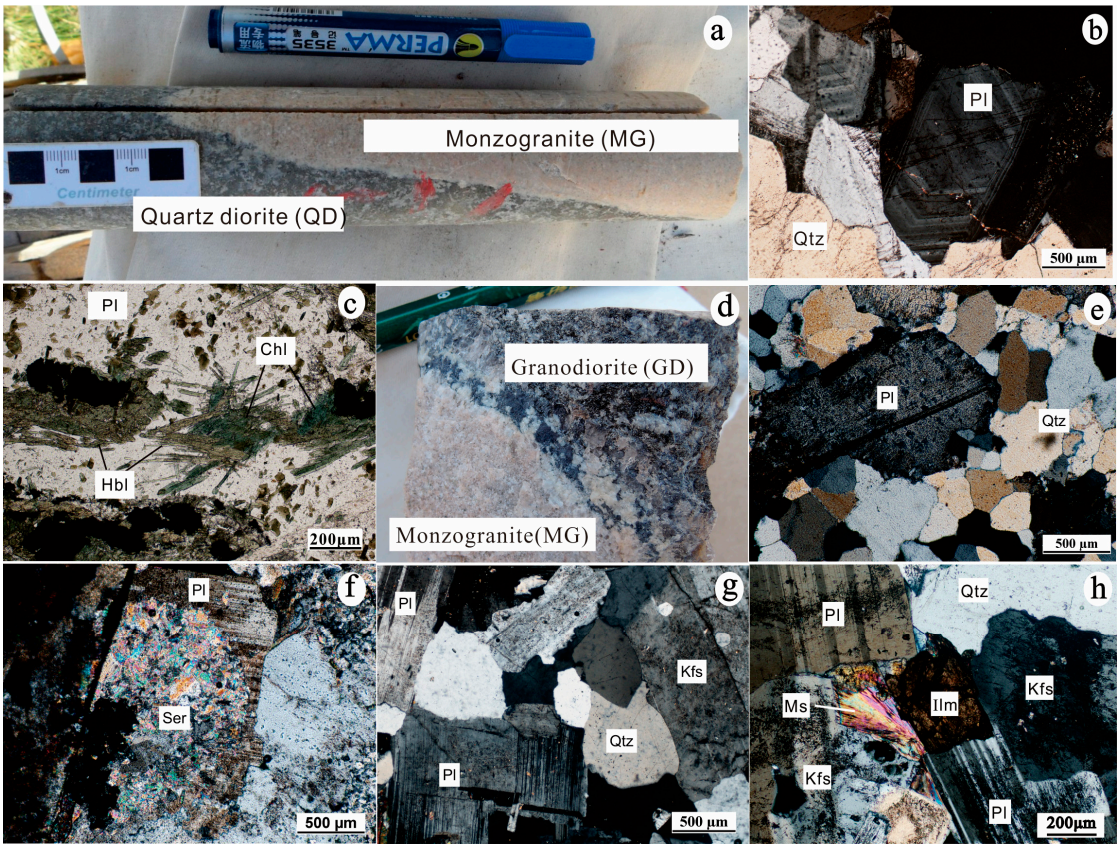

Figure 3. Hand samples (**a**,**b**) and photomicrographs (plane and cross polarized transmitted light, PPL & CPL) (**c**–**h**) of the intrusive rocks from the Wulandele molybdenum deposit. (**a**) Quartz diorite (QD) intruded by the fine-grained monzogranite (MG); (**b**) Zonal texture of the plagioclase in the fresh QD (CPL); (**c**) Chlorite alteration in the QD (PPL); (**d**) Granodiorite (GD) intruded by the MG; (**e**) Photomicrograph of the fresh GD (CPL); (**f**) Sericitization in the GD (CPL); (**g**) Photomicrograph of the fresh MG (CPL); (**h**) Muscovite alteration in the MG with the accessory mineral of ilmenite (CPL). Abbreviations: Qtz—quartz, Pl—plagioclase, Kfs—alkali feldspar, Hbl—Hornblende, Chl—Chlorite, Ser—Sericite, Ilm—Ilmenite.

The Mo mineralization styles are disseminated, veinlet-disseminated, and veined mineralization (Figure 4a–f). The disseminated mineralization is distributed in the inner contact zone of the MG; veinlet-disseminated and veined mineralization types are mainly distributed in the cracks of the surrounding rocks (the QD and GD). The hydrothermal alteration includes potassic alteration, silicification, greisenization, argillic alteration, and propylitic alteration. In the hydrothermal mineralization stage, the metallic minerals are mainly molybdenite, chalcopyrite, and pyrite, with minor sphalerite, magnetite, and stibnite (Figure 4g–i). Nonmetallic minerals include alkali feldspar, quartz, sericite, muscovite, fluorite, chlorite, epidote, and calcite. Ore textures include automorphic and xenomorphic texture, interstitial texture, intergrowth texture, metasomatic texture, etc. The alteration zones of the Wulandele Mo deposit are, successively, potassic zone, quartz sericitization zone, and the propylitic zone, from inside to outside. The mineralization process can be divided into four stages: (1) quartz–alkali feldspar–magnetite stage, (2) quartz–molybdenite–pyrite stage, (3) quartz–muscovite–polymetallic sulfide stage, and (4) quartz–carbonate–fluorite stage. The main Mo-mineralized stage is the quartz–molybdenite–pyrite stage.

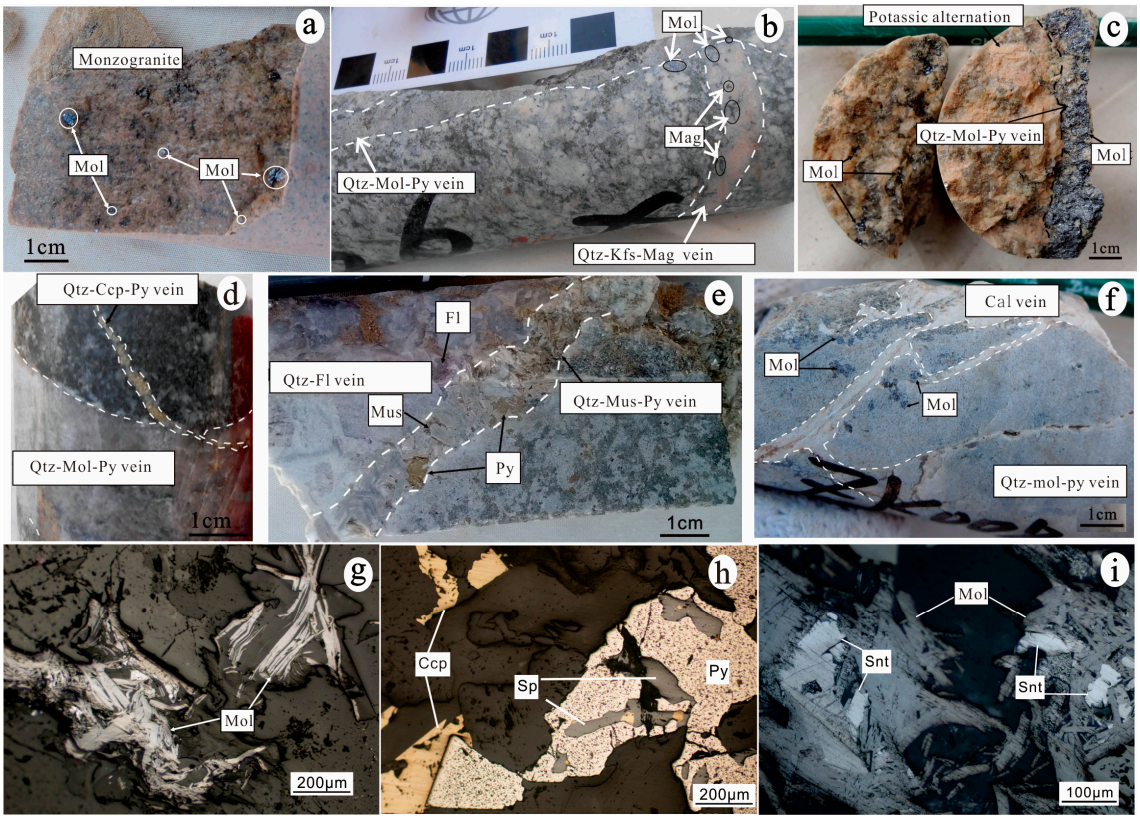

Figure 4. Photographs and photomicrographs of the ores and metallic minerals from the Wulandele molybdenum deposit. (**a**) Disseminated mineralization of monzogranite; (**b**) Quartz–alkali feldspar –magnetite vein intruded by quartz–molybdenite–pyrite vein; (**c**) Potassic alternation and quartz–molybdenite–pyrite vein; (**d**) Quartz–molybdenite–pyrite vein intruded by quartz–chalcopyrite–pyrite vein; (**e**) Quartz–fluorite vein intruded into quartz–Ms–pyrite vein; (**f**) Quartz–molybdenite–pyrite vein intruded by calcite vein; (**g**) Molybdenite occurring as aggregated flakes in monzogranite (reflected light); (**h**) Pyrite, chalcopyrite, and sphalerite in ores (reflected light); (**i**) Paragenetic stibnite and molybdenite (reflected light). Abbreviations: Mol—molybdenite, Ccp—chalcopyrite, Py—pyrite, Sp—sphalerite, Snt—stibnite, Mag—magnetite, Qtz—quartz, Kfs—alkali feldspar, Fl—Fluorite, Mus—muscovite.

3. Samples and Analytical Methods

The Re-Os model age of molybdenite, bulk rock major and trace elements of the MG, Rb-Sr, Sm-Nd, and Pb isotopes of the MG were carried out in this research. All samples of the MG and molybdenite were collected from the drill cores in the Wulandele Mo deposit. All the bulk rock samples for these analyses were fresh or least-altered rocks.

3.1. Re-Os Model Age of Molybdenite

One sample of the Re-Os model age of molybdenite was collected from the drill (XA10-607). We first selected the fine-grained, fresh (without oxidation), and non-contaminated molybdenite assemblages, and crushed and separated to obtain monomineralic molybdenite with purity over 99% for molybdenite Re-Os dating. The Re-Os isotope analyses were carried out in the Re-Os laboratory at the National Research Center of Geoanalysis, Chinese Academy of Geological Sciences, Beijing. The details of the Re-Os chemical separation procedures have been described by Du et al. [15]. Rhenium and Os isotope ratios were determined by a TJA X-series inductively coupled plasma-mass spectrometer (ICP–MS). During this study, Re blanks were < 0.0067 ng and Os blanks were <0.0008 ng. The uncertainty for each individual age determination was 1.4%, including the uncertainties for the ^{187}Re decay constant, isotope ratio measurements, and spike calibrations. The model ages were calculated using the following formula: $t = \ln(^{187}Os/^{187}Re + 1)/\lambda$. A ^{187}Re decay constant of 1.666×10^{-11} y^{-1} (±1.02%) was used [16].

3.2. Major and Trace Element Analyses

Six samples of the MG were prepared for bulk rock major and trace element analysis. The major elements were analyzed by X-ray fluorescence spectrometry (XRF) at the ALS Chemex Laboratory, and the accuracy and precision of the XRF analyses were estimated to be within 5%. The ferrous oxide (FeO) was analyzed for all samples by acid digestion and potassium dichromate titration. Trace element analyses were determined by ICP-MS (Perkin Elmer Elan 9000 and Agilent 7700× with a shielded torch) after fusion and then multi-acid digestion of the samples, and the accuracy and precision were estimated to be better than 10%.

3.3. Sr–Nd–Pb Isotopes

Four samples were selected for Sr, Nd, and Pb isotope ratio analysis. The bulk rock Sr-Nd isotopes were determined by Phoenix thermal ionization mass spectrometry, and the bulk rock Pb isotopes were determined by Isoprobe-T thermal ionization mass spectrometry at the Beijing Research Institute of Uranium Geology (BRIUG). The 100 mg sample powders were dissolved in HF + HNO_3 + $HClO_4$ mixture and separated using the conventional cation-exchange technique with HCl as eluent for Sr and Nd, and using strong alkali anion exchange resin with HBr and HCl as eluents for Pb.

The $^{143}Nd/^{144}Nd$ ratios were normalized to $^{146}Nd/^{144}Nd_{standard} = 0.7219$, while the $^{87}Sr/^{86}Sr$ ratios were normalized with $^{88}Sr/^{86}Sr_{standard} = 0.1194$ as the internal standard. The NBS 987 Sr standard yielded $^{87}Sr/^{86}Sr$ ratios of 0.710250 ± 7 (2δ) and JMC Nd Standard gave $^{143}Nd/^{144}Nd$ ratios of 0.512109 ± 3 (2δ). For Pb isotope analyses, sample powders were spiked and dissolved in concentrated hydrofluoric acid and separated and purified by the conventional anion-exchange technique. Repeated analyses of the NBS981 standard yielded $^{204}Pb/^{206}Pb = 0.0591107 \pm 2$, $^{207}Pb/^{206}Pb = 0.914338 \pm 7$, and $^{208}Pb/^{206}Pb = 2.164940 \pm 15$.

4. Results

4.1. Molybdenite Re-Os Geochronology

The Re-Os isotope results are listed in Table S1. The total Re and normal Os are 31.82 ppm with an uncertainty of 0.24 and 0.2757 ppb with an uncertainty of 0.02, respectively. The ^{187}Re and ^{187}Os concentrations are 20 ppm with an uncertainty of 0.15 and 44.98 ppb with an uncertainty of 0.40,

respectively. The Re-Os model age is 134.8 ± 1.9 Ma, which is consistent with the isochron age of 134.1 ± 3.3 Ma reported by Tao et al. [1]. Thus, the Mo mineralization age of the Wulandele Mo deposit can be considered as early Cretaceous.

4.2. Major and Trace Element Compositions

The major element compositions are presented in Table S2. The MG has high SiO_2 (71.7 to 73.8 wt.%), Na_2O (3.76 to 4.01 wt.%), K_2O (4.7 to 4.96 wt.%), and low CaO (0.92 to 1.22 wt.%), MgO (0.27 to 0.37 wt.%), P_2O_5 (0.05 to 0.07 wt.%), and TiO_2 (0.17 to 0.22 wt.%). All samples fall in the granite field in the total alkali silica (TAS) diagram, and high-K calc-alkalic series in the K_2O vs. Si_2O diagram (Figure 5). This rock has moderate Al_2O_3 (13.65 to 14.30 wt.%) and A/CNK values of 1.03 to 1.05, indicating a weakly peraluminous composition. The rock has MgO contents of 0.27 to 0.37 wt.% and $Mg^{\#}$ of 23.3 to 26.88. In the Harker diagrams of major elements (Figure 6), most compatible major elements show a decrease in content coincident with increasing SiO_2 content, except K_2O content, which increases with increasing SiO_2 content. Using the bulk rock Zr composition to represent the melt composition in the model [17], zircon saturation temperatures (T_{Zr}) were calculated for the MG (Table S2). The calculated results show the MG has a mean T_{Zr} of 778 °C (760 to 786 °C).

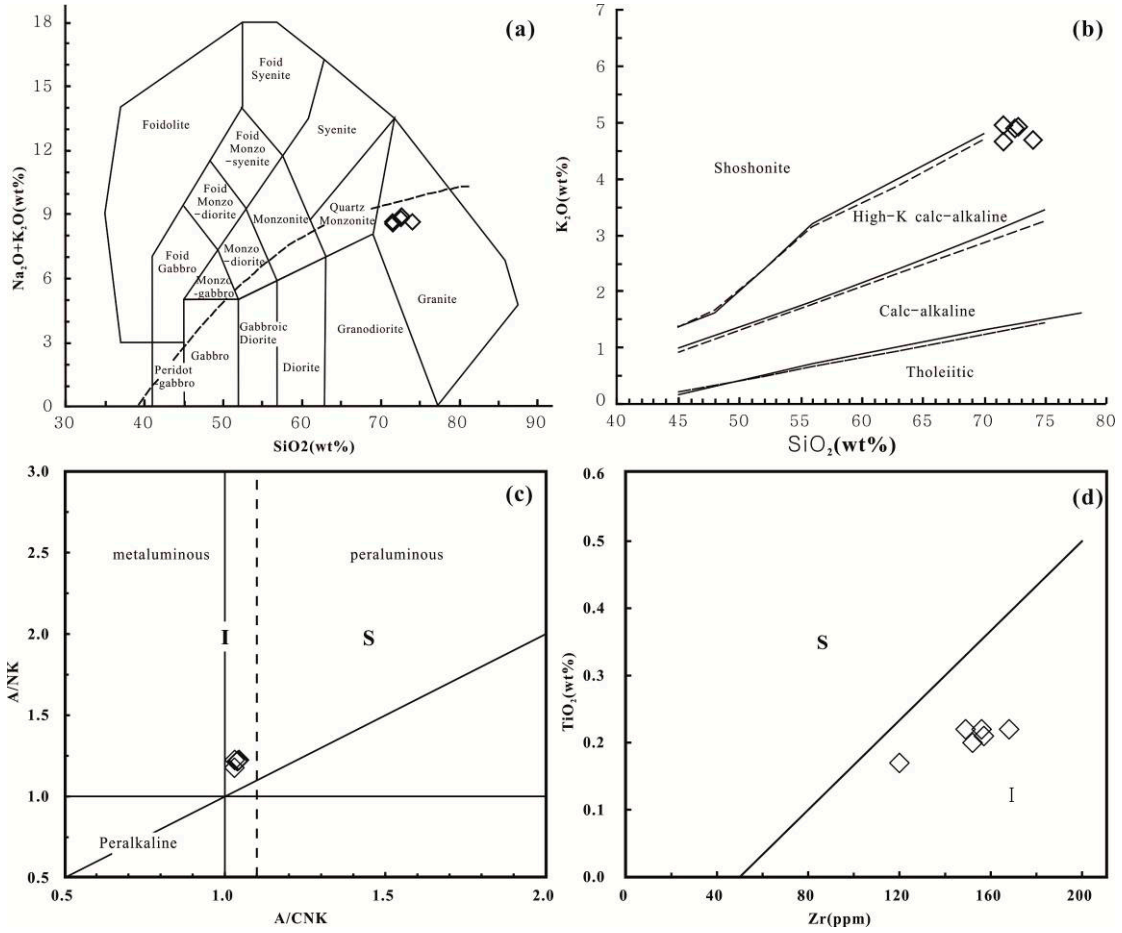

Figure 5. TAS (**a** after [18]), K_2O vs. SiO_2 diagram (**b** after [19]), $Al_2O_3/(CaO + Na_2O + K_2O)$ vs. $Al_2O_3/(Na_2O + K_2O)$diagram (**c** after [20]) and TiO_2 vs. Zr diagram (**d**) for the MG from the Wulandele Mo deposit. S, S-type granite; I, I-type granite.

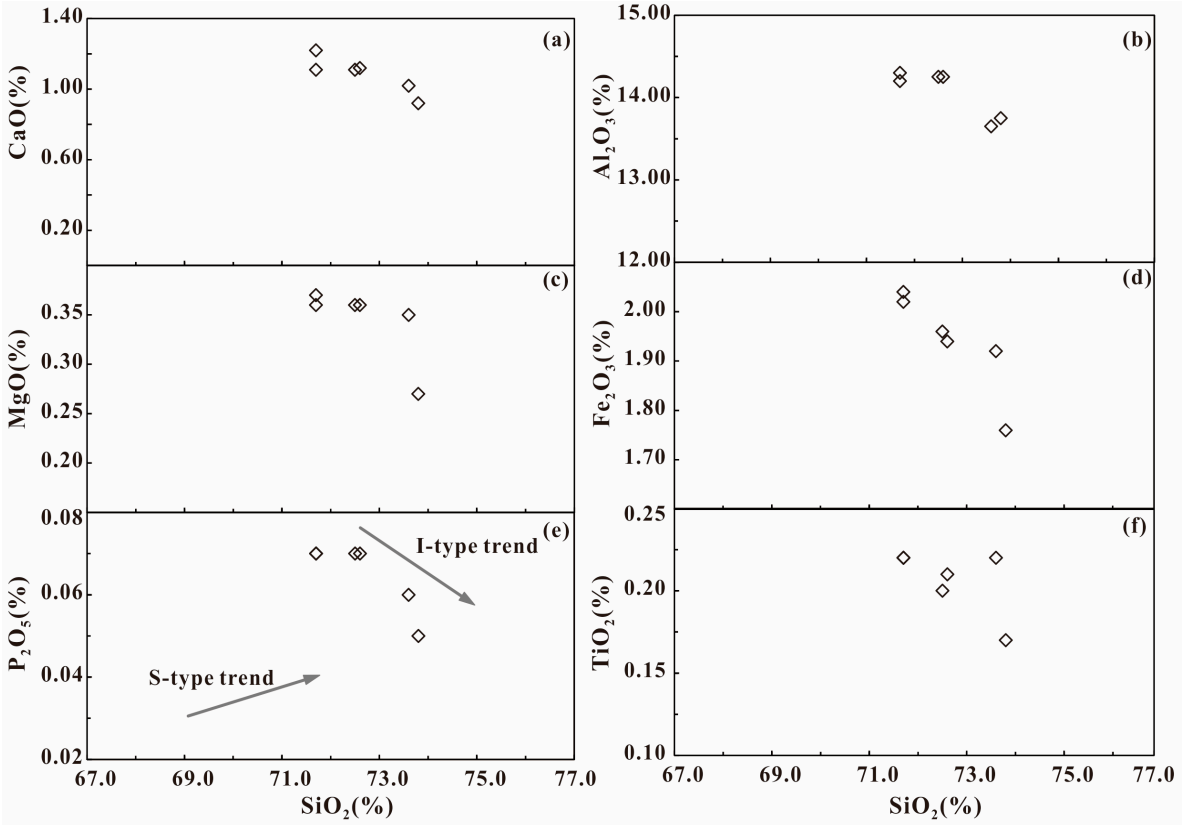

Figure 6. Harker diagrams of major elements for the MG from the Wulandele Mo deposit: (**a**) CaO vs. SiO_2; (**b**)Al_2O_3 vs. SiO_2; (**c**) MgO vs. SiO_2; (**d**) Fe_2O_3 vs. SiO_2; (**e**) P_2O_5 vs. SiO_2; (**f**) TiO_2 vs. SiO_2.

The results of trace elements analysis are listed in Table S3. The data show that the MG is characterized by fairly low concentrations of Ba, Sr, Nb, P, and Ti and elevated concentrations of Rb, K, and U (Figure 7a). The chondrite-normalized REE patterns of the MG (Figure 7b) are subparallel, showing relative enrichment of light rare earth elements (LREE) and depletion of heavy rare earth elements (HREE), with $(La/Yb)_N$ values from 14.96 to 44.64, and moderate negative Eu anomalies (range from 0.38 to 0.57).

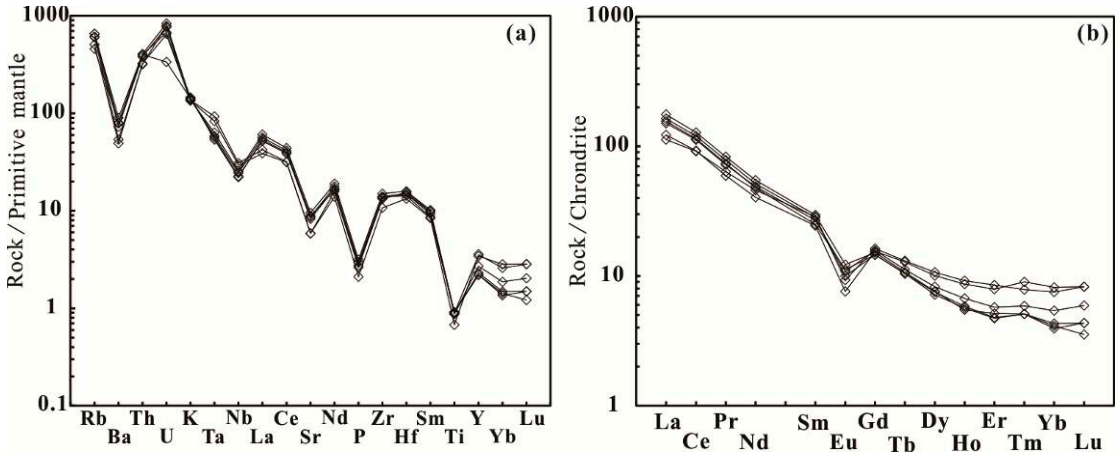

Figure 7. Primitive mantle-normalized trace element spider diagram (**a**) and chondrite-normalized REE diagram (**b**) for the MG from the Wulandele Mo deposit. The primitive mantle data are from [21], the chondrite-normalized data are from [22].

4.3. Bulk Rock Sr-Nd-Pb Isotopes

Bulk rock Sr-Nd-Pb isotopic compositions of the MG and the calculation parameters are listed in Table S4. Initial $^{143}Nd/^{144}Nd$ ratios and $\varepsilon_{Nd}(t)$ were calculated using the average crystallization age 131.3 Ma [1]. The Rb/Sr ratios for all samples are below or near 3.0, suggesting that they can be used in the calculation of $(^{87}Sr/^{86}Sr)_i$ values and petrogenetic discussion [23,24]. The MG exhibits homogeneous Sr and Nd isotopic compositions, with $(^{87}Sr/^{86}Sr)_i$ = 0.705347–0.705771 and $(^{143}Nd/^{144}Nd)_i$ = 0.512366–0.512400. The $\varepsilon_{Nd}(t)$ of MG varies from −2.0 to −1.3, and the depleted mantle Nd model ages (T_{DM}) range from 921 to 1047 Ma.

Bulk rock Pb isotopic compositions (Table S4) show the MG has present-day $^{206}Pb/^{204}Pb$ ranging from 18.228 to 19.014, $^{207}Pb/^{204}Pb$ ranging from 15.510 to 15.562, and $^{208}Pb/^{204}Pb$ ranging from 38.015 to 38.448. The initial Pb isotopic ratios were calculated by the average crystallization age of 131.3 Ma using the Geokit geochemical toolkit designed by Lu [25]. The results suggest that the MG has initial Pb isotopic ratios of $(^{206}Pb/^{204}Pb)_t$, $(^{207}Pb/^{204}Pb)_t$, and $(^{208}Pb/^{204}Pb)_t$ are 17.5673 to 18.3676, 15.4778 to 15.5271, and 37.5036 to 37.9423, respectively.

5. Discussion

5.1. Mo Mineralization Age and Ore-Related Instrusion

The molybdenite Re-Os isotopic model age of 134.8 ± 1.9 Ma from the Wulandele deposit is consistent with the Re-Os isotopic isochron age of 134.0 ± 4.2 Ma and weight mean age of 134.1 ± 3.3 Ma reported by Tao et al. [1], within uncertainties. Thus, we suggested that the Mo mineralization age of the Wulandele Mo deposit can be considered as early Cretaceous.

Tao et al. [1,6] reported the zircon U-Pb ages of the QD and GD are 292.6 ± 0.5 Ma and 299.3 ± 2.4 Ma, respectively, indicating that the QD and GD are the wall rocks for the Mo mineralization. The MG has the zircon U-Pb age of 131.3 ± 1.6 Ma, suggesting its intimately temporal relationship with Mo mineralization. Furthermore, the geological investigations show that the disseminated Mo mineralization mainly occurs inner to the MG or along the contact zones between the MG and its wall rocks (QD and GD), which implies that the MG has a closer spatial relationship with Mo mineralization.

Thus, we argue that the Mo mineralization of Wulandele deposit occurred during the early Cretaceous and is genetically associated with the MG intruding the QD and GD, which are just wall rocks hosting parts of Mo-mineralized veins.

5.2. Petrogenesis of the MG

The contents of CaO, Al_2O_3, MgO, and total Fe_2O_3 decrease with increasing SiO_2 contents in the MG (Figure 6), indicating that fractional crystallization has occurred in the magmatic process. The trends are consistent with the fractionation of Al-, Fe-, Ca-, and Mg-rich phases, such as hornblende and plagioclase.

The MG has relatively lower values of Zr + Nb + Y + Ce (214.1–274.4 ppm), and falls in the field of FG (fractionated felsic granite) in the FeO_T/MgO vs. (Zr + Nb + Ce + Y) and $(K_2O + Na_2O)$/CaO vs. (Zr + Nb + Ce + Y) diagrams (Figure 8a,b), which suggests that it experienced relatively high degrees of fractional crystallization. All samples have low A/CNK of 1.03–1.05 (all < 1.1, Figure 5c), and fall in the I-type granite field in both the A/NK vs. A/CNK diagram and the TiO_2 vs. Zr diagram (Figure 5d) indicating its I-type granitic affinity, which is consistent with the variation trend of P_2O_5 vs. SiO_2 (Figure 6e). Although slightly higher, the 10,000×Ga/Al values are very close to 2.6, which is the boundary of S-, I-, and A-type granites (Figure 8c,d) [26]. Thus, we argued that the MG is a highly fractionated I-type granite.

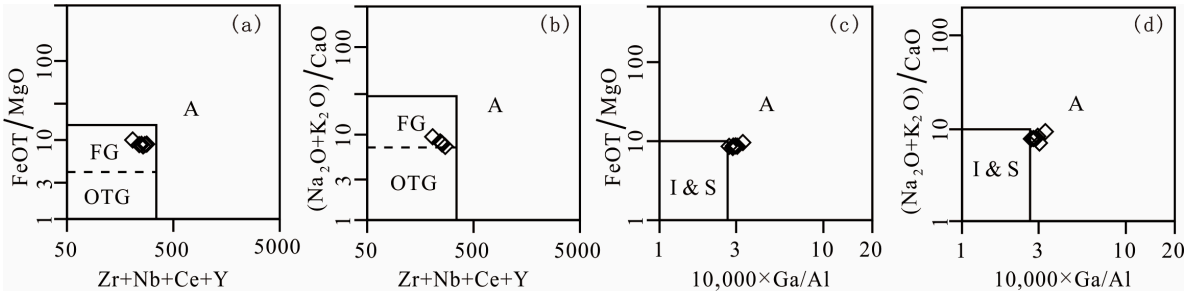

Figure 8. Discrimination diagrams of granite type for the MG from Wulandele Mo deposit: (**a**) FeOT/MgO vs. Zr + Nb + Ce + Y; (**b**) (Na_2O + K_2O)/CaO vs. Zr + Nb + Ce + Y; (**c**) FeOT/MgO vs. 10,000×Ga/Al; (**d**) (Na_2O + K_2O)/CaO vs. 10,000×Ga/Al. FG—Fractionated Granite; OGT—unfractionated M-, I-, and S-type granites; A—A-type granite (after [26]).

The features of high-silica, high-K_2O, and low-CaO, high-K calc-alkaline series, weakly peraluminous, suggest that the MG can be classified as K-rich and alkali feldspar porphyritic calc-alkaline granitoids (KCG), as defined by Barbarin [27,28]. This is also supported by its characteristics of enriched Rb, U, Th and K, depleted Ba, Sr, Nb, P and Ti, and right-sloping chondrite-normalized REE pattern. These features implied the MG might originate from a mixed source that involved both the mafic juvenile lower continental crust (mantle-derived materials) and older continental-crustal materials, which are consistent with its mixed Sr and Nd isotope features.

The MG has the characteristics of lower initial $^{87}Sr/^{86}Sr$ ratios (0.705347 to 0.705771), weak negative $\varepsilon_{Nd}(t)$ (−2.0 to −1.3). All samples of MG fall between the "depleted mantle" and "lower continental crust" fields in the $\varepsilon_{Nd}(t)$ vs. $(^{87}Sr/^{86}Sr)_i$ diagram (Figure 9a, [23]), indicating multiple contributions from juvenile mafic lower continental crustal components and ancient metamorphic basement with possible slight contamination of upper continental crust. All samples plot within the field of basaltic magma in the $(^{87}Sr/^{86}Sr)_i$ vs. t diagram, further supporting this model (Figure 9b). Furthermore, according to the mixing calculation using different end members (Figure 9a, [23]), the source of MG includes mainly juvenile mafic lower continental crust (or depleted mantle) components (60–70%) with minor ancient continental crust (30–40%).

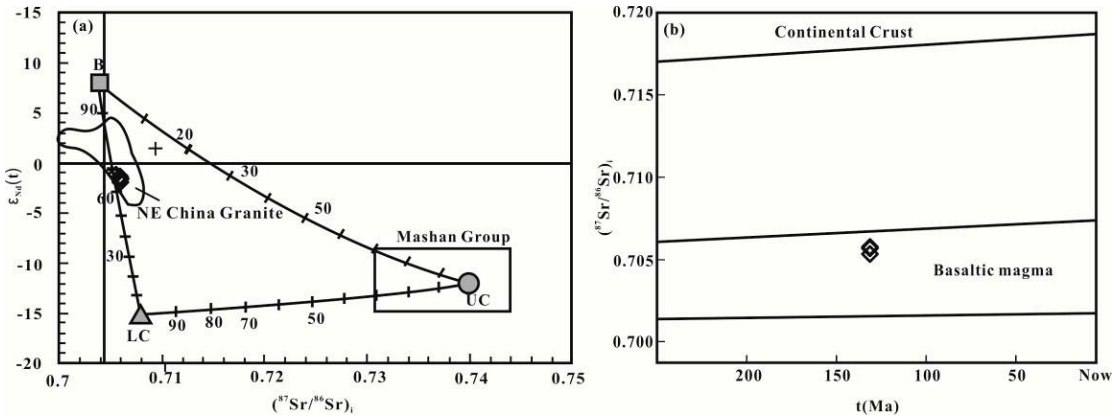

Figure 9. $\varepsilon_{Nd}(t)$ vs. $(^{87}Sr/^{86}Sr)_i$ (**a**) and $(^{87}Sr/^{86}Sr)_i$ vs. t (**b**) for the MG from the Wulandele Mo deposit. The field for NE China Granite is from [23]. The calculated parameters of Nd (ppm), $\varepsilon_{Nd}(t)$, Sr (ppm), and $(^{87}Sr/^{86}Sr)_i$ are 15, +8, 200, and 0.704 for basalt; 30, −12, 250, and 0.740 for upper continental crust (UC); 20, −15, 230, 0.708 for lower continental crust (LC). All end-number data derive from [23].

In the plot of the Pb isotope evolution curves (Figure 10), the samples fall in the field between the typical mantle and orogenic belts in the $^{207}Pb/^{204}Pb$ vs. $^{206}Pb/^{204}Pb$ diagram (Figure 10a), and the vicinity of the oceanic island volcanic and orogenic belts in the $^{208}Pb/^{204}Pb$ vs. $^{206}Pb/^{204}Pb$ diagram (Figure 10b), indicating that the source of MG melt is closely related to the mixed origin of the mantle and continental crustal contribution. Combined with the above discussion, we argue that the MG melt originated from a contribution of the predominantly mafic juvenile lower continental crust partial melts (or depleted mantle) with the possible minor ancient continental crust, and possibly contaminated by upper continental crust during melt ascent.

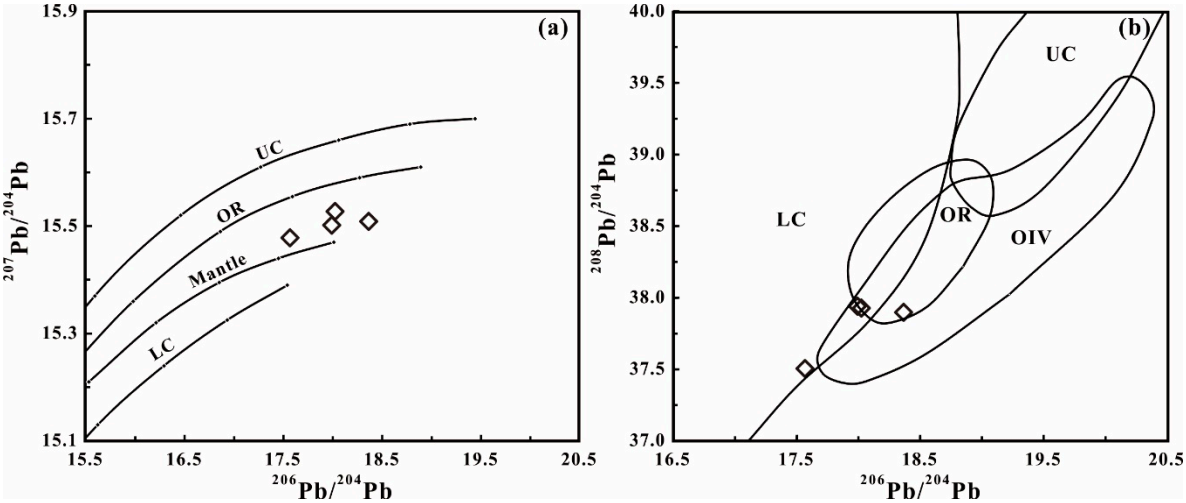

Figure 10. $^{207}Pb/^{204}Pb$ vs. $^{206}Pb/^{204}Pb$ (**a**) and $^{208}Pb/^{204}Pb$ vs. $^{206}Pb/^{204}Pb$ (**b**) diagrams of the Wulandele MG with Pb isotopic evolution curves (after [29]). UC—Upper Crust; LC—Lower Crust (both continental crust); OR—Orogenic Belt; OIV—Oceanic Island Volcanic.

5.3. Tectonic Implications

The genesis of the different types of granitoid is strongly constrained by the geodynamic environment. KCG could present in various geodynamic environments, such as the periods of relaxation that separate periods of culmination within a collision event, or transition from a compressional regime to an extensional regime [27,28].

In the Rb vs. Y + Nb diagrams (Figure 11a; [30,31]), the MG occurred in the domain of syn-collisional granite and post-collisional granite. In the Rb/30-Hf-3Ta ternary plot ([32]) (Figure 11b,c), the MG also falls in the vicinity of the syn-collisional domain to the late- and post-collisional domain. Meanwhile, in the R1-R2 ([32]) diagrams, the MG samples show a closer relation to a late orogenic affinity. All these geochemical affinities suggest that the MG probably formed in an extensional environment, which is related to collapse or delamination of the thickened lithosphere post-collisional tectonic setting that was probably affected by local stretching within the syn-collisional setting.

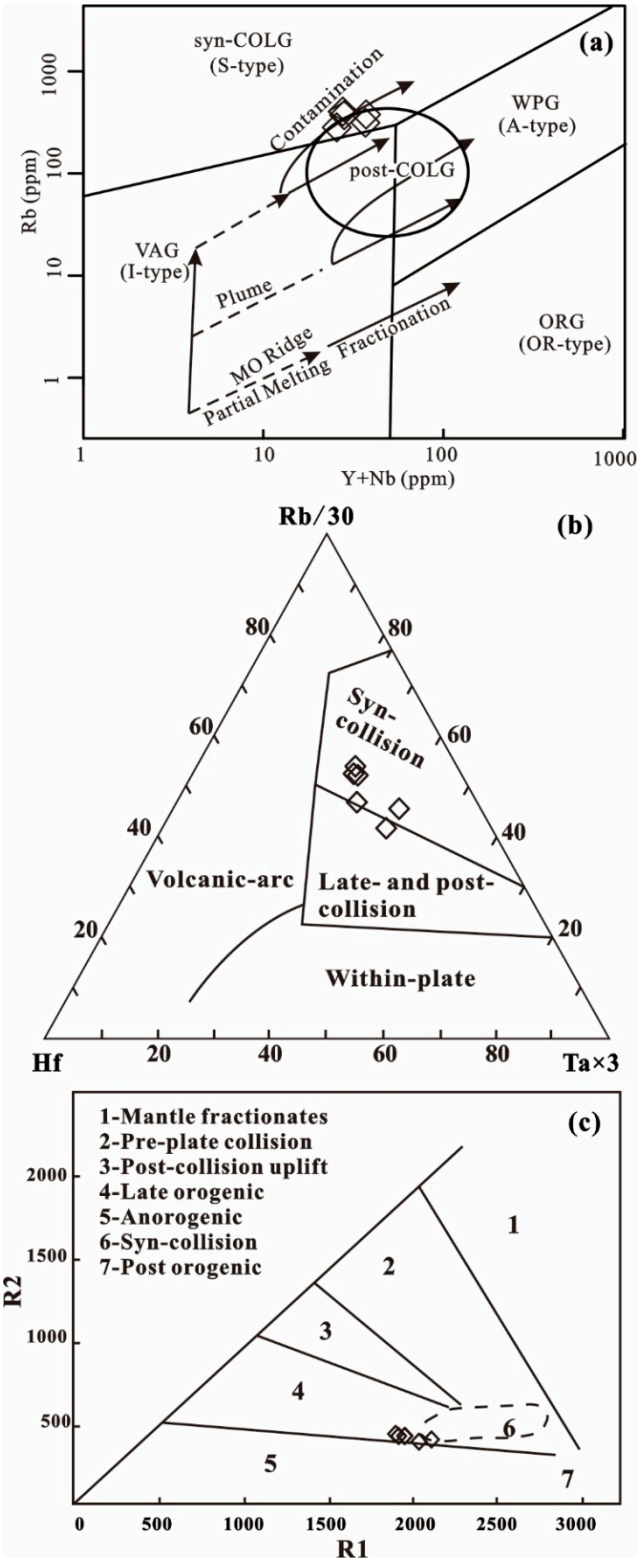

Figure 11. Tectonic discrimination diagrams for granitoid rocks with MG samples plotted from the Wulandele Mo deposit (**a** after [30,31]; **b** after [32]; **c** after [33]); VAG, Volcanic arc granites; Syn-COLG, Syn-collisional granites; WPG, Within-plate granites; ORG, Ocean ridge granites; post-COLG, post-collisional granites.

Two geodynamic processes play important roles in the formation of granites in XMOB during Jurassic to Cretaceous; one is the closure of the Mongol–Okhotsk ocean, and another is the western subduction of the Paleo-Pacific plate. Although there is controversy concerning the closure time and style of the Mongol–Okhotsk ocean, an increasing number of researchers have come to a consensus that the closure of the Mongol–Okhotsk ocean was a scissor-like closure (diachronous) from the west (Mongolia) in the Triassic or Jurassic to the east (Amur) in the Early Cretaceous [34–41], which is consistent with the post-collision setting suggested by MG located near the west Mongol–Okhotsk tectonic belt during the early Cretaceous (131 Ma). However, the affinity of the syn-collision setting indicated the MG was also likely related to local extension associated with western subduction of the Paleo-Pacific plate. Therefore, we suggested that the MG formed mainly in response to post-orogenic extensional collapse or delamination of the thickened lithosphere of the Mongol–Okhotsk belt, weakly coupled with local extension related to Paleo-Pacific plate subduction.

5.4. Formation of Mo Mineralization

Redox condition seems to be a crucial factor that affects the behavior of Mo as a highly incompatible element, with highly oxidizing magma conditions considered to be beneficial to the formation of porphyry Mo deposits ([42,43]). The ΔOx values ($\Delta Ox = \log_{10}(Fe_2O_3/FeO) + 0.3 = 0.03TFeO$) of the MG (−0.11 to 0.04) are near 0, which is considered a critical value of oxidized and reduced granites [44]. Half the samples fall into the moderately oxidized field, and the other half of the samples fall into the moderately reduced field (Figure 12a; [44]), indicating that the MG mainly shows weakly oxidized to weakly reduced features. Furthermore, the values of Fe_2O_3/FeO for all samples are in the range of 0.35 to 0.49, which is below 0.5, suggesting that the MG can be classified into the ilmenite series rather than the magnetite series (Figure 12b; [45]). These features imply that the MG does not seem to have the characteristics of high oxidization, although analysis of ferrous iron from disseminated pyrite would skew the interpretation of the abundance of FeO. However, it may appear that the highly oxidative magma may not be necessary for the formation of porphyry Mo deposits, and weakly oxidizing magma can also form Mo deposits; caution should be used in interpretation of Fe_2O_3/FeO alone.

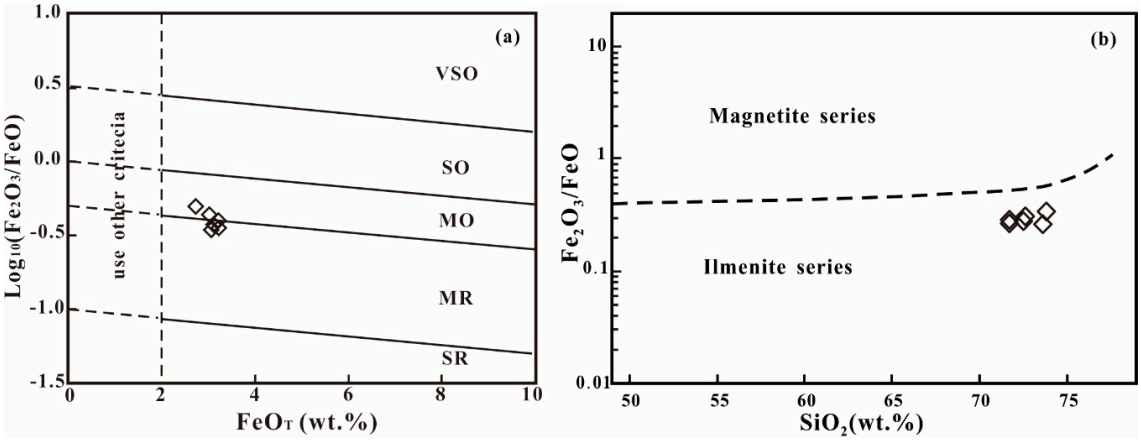

Figure 12. Redox classification scheme for the MG from Wulandele Mo deposit (**a** after [44]; **b** after [45]). FeO_T refers to the total Fe in the sample reported as FeO (total). VSO—very strongly oxidized, SO—strongly oxidized, MO—moderately oxidized, MR—moderately reduced, SR—strongly reduced.

Crystal fractionation is an important evolved process for examining the association of ore with felsic magmatism. The role of magmatic fractionation can be seen in association of Cu porphyry deposits with the lower fractionated and most oxidized rocks, the association of W deposits with moderately fractionated rocks, and of Mo and Sn with the most highly fractionated rocks [31,46,47]. The Mo to Cu ratio of the Wulandele molybdenum deposit is remarkably high (up to 39.2 [1]). This copper-poor character is compatible with the ore mineral assemblage of the Wulandele molybdenum deposit, which

has very limited chalcopyrite in the deposit according to field and microscopic observations (Figure 4). As a copper-poor stock, the MG represents an obviously highly fractionated feature, defined by very low abundance of ferromagnesian and Ca-rich minerals. Biotite is the major mafic mineral of the MG, and it comprises less than 3% of the total volume of the rock (Figure 3g,h). Copper and Au tend to be depleted during fractional crystallization of mafic minerals [48], therefore extensive magma (crystal) fractionation resulted in copper depletion compared with molybdenum in the Wulandele deposit. This relationship is also evident in the fractionation diagram with an evolved granitic composition (Figure 13).

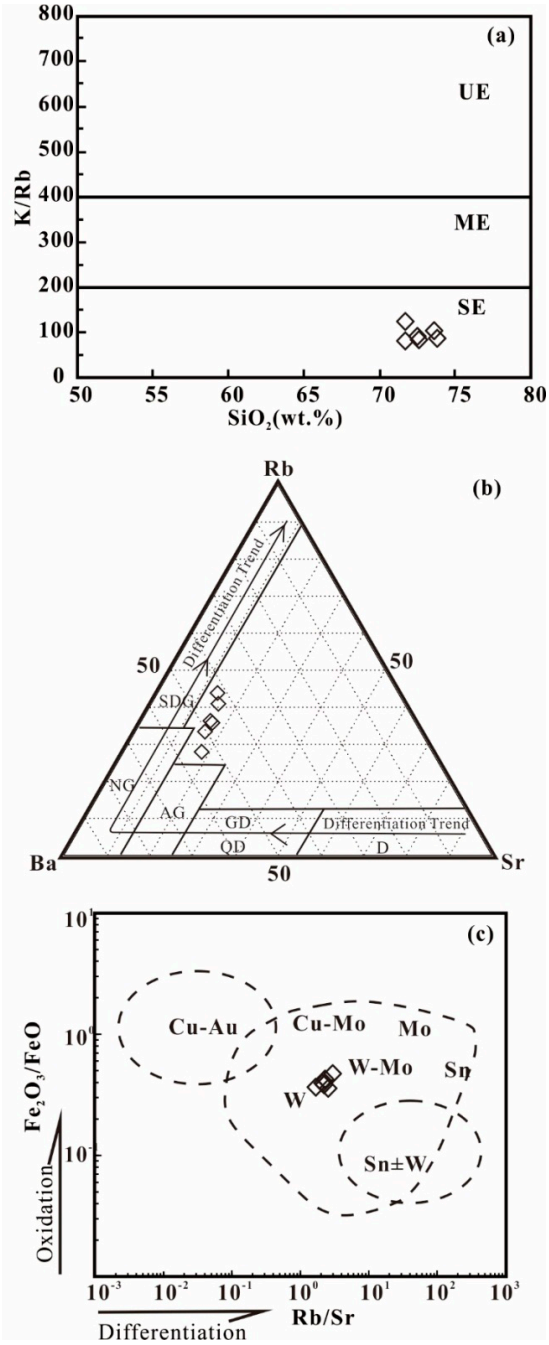

Figure 13. K/Rb vs. SiO_2 (**a** after [44]), Rb-Ba-Sr ternary diagram (**b** after [49]), and Fe_2O_3/FeO vs. Rb/Sr (**c** after [45,50]) diagrams for the MG from Wulandele Mo deposit. UE—Unevolved, ME—Moderately evolved, SE—Strongly evolved; D—Diorites, QD—Quartz Diorites, GD—Granodiorites, NG—Normal Granites, SDG—Strongly Differentiated Granites, AG—Anomalous Granites.

Blevin [44] have suggested that K/Rb is an effective proxy to discriminate the evolved degree for the felsic melt, and the magma can be considered to experience a strong fractionation process when its K/Rb ratio is below 140. The MG had a K/Rb value of 82.5 to 125.2, with an average of 96.19, and all samples fall in the strongly evolved field in the K/Rb vs. SiO_2 diagram (Figure 13a), which indicates that the MG was undergoing a strong process of fractionation, favorable to Mo mineralization. Barium and Sr are more compatible, so also appear to be specifically sensitive indicators for tracing possible differentiation trends [49]. Within the Rb-Ba-Sr ternary diagram (Figure 13b), the samples are near the field of strongly differentiated granites, which suggest that the MG has experienced a strong differentiation. In the Fe_2O_3/FeO vs. Rb/Sr diagram (Figure 13c, [50]), the samples of MG fall in the Mo-W mineralization area, also indicating that the MG is a Mo-favourable intrusion.

In the XMOB, most Cretaceous intermediate-felsic intrusions are cooper-infertile and Mo-favorable. The granitoids related to Mo mineralization mainly occurred during the late Jurassic to early Cretaceous, whereas the granitoids related to Cu (Mo) or Mo (Cu) mineralization mainly occurred in earlier ages, such as Duobaoshan granodiorite porphyry (477 Ma, Ordovician), Wunugetushan monzogranite porphyry deposit (Cu-Mo mineralization, 188 Ma, Early Jurassic), and Zhunsujihua granodiorite and leucogranite (Mo-Cu mineralization, 299–300 Ma, late Carboniferous) [4,6,51,52]. In the Dalaimiao area, besides 39.2 for the Wulandele deposit, the Mo/Cu value is 48.6 for the Wurinitu deposit, as another large Mo deposit formed during the early Cretaceous. As for the Zhunsujihua Mo deposit formed in the late Carboniferous to early Permian, the value is as low as 6.7 [5]. Thus, we deduce that the older intermediate-felsic intrusions (such as Ordovician to early Jurassic) are more favorable to form Cu mineralization, while the younger intrusions are more favorable to form Mo mineralization (such as early Cretaceous) in the Dalaimiao area.

6. Conclusions

From the above discussion, conclusions are summarized as follows:

(1) Both the temporal and spatial relationship between the Mo mineralization and the intrusive rocks suggest that the MG is the ore-related intrusion, and the QD and GD are just ore-hosted wall rocks that host parts of those Mo-mineralized veins.

(2) The MG is classified as a high-K, calc-alkaline granitoid, with A/CNK < 1.1, quite low I_{Sr}, and relatively high $\varepsilon_{Nd}(t)$ values. The geochemical features constrain the MG to be highly evolved I-type granite, which indicates that its source magma originated by partial melting of a mixed source, including depleted mantle and a lower continental crustal source, possibly contaminated by assimilation of upper continental crust during ascent.

(3) The geological and geochemical features imply that the MG and Mo mineralization formed mainly in response to post-orogenic extensional collapse or delamination of the thickened lithosphere of the Mongol–Okhotsk belt, weakly coupled with local extension related to Paleo-Pacific plate subduction.

(4) The MG shows weakly oxidized to weakly reduced features, indicating that the highly oxidative magma maybe not be absolutely necessary for formation of a porphyry Mo deposit, although it is important to be aware of the effect of iron sulfides affecting the ferric/ferrous analyses. The process of extensive fractional crystallization is critical to Mo fertility in this evolved magmatic-hydrothermal system.

(5) The relationship of mineralized elements with fractionation degrees and intrusion ages in the Dalaimiao area suggest that exploration for Mo deposits should focus on Cretaceous granitoids, while for Cu deposits exploration should focus the Ordovician to Carboniferous intermediate-felsic stocks in the Dalaimiao area.

Supplementary Materials: The following are available online at http://www.mdpi.com/2075-163X/10/4/374/s1, Table S1: Re-Os data for molybdenite samples from the Wulandele Mo deposit; Table S2: Major element contents and relative parameters of the MG from the Wulandele Mo deposit; Table S3: Trace element contents and relative parameters of the MG from the Wulandele Mo deposit; Table S4: Sr-Nd-Pb isotopic compositions of the MG from the Wulandele Mo deposit [25,53].

Author Contributions: Conceptualization, X.Z. and C.Y.; Funding acquisition, Z.Z.; Investigation, Y.Q., Y.W., F.Z., Z.Y., and R.L.; Methodology, Y.Q.; Writing—original draft, X.Z. and C.Y.; Writing—review & editing, D.R.L. All authors have read and agreed to the published version of the manuscript.

Funding: This research was funded by the program of China Geological Survey (12120113089300, 12120113088800, 12120113079400).

Acknowledgments: We appreciate the engineers of Geological Survey Institute of Inner Mongolia Autonomous Region for their help in the fieldwork. Hengsheng Shang, Qidong Xu, and Qinglin Xia are thanked for their help and fruitful discussion. We are also grateful to three reviewers for their constructive comments. D.R.L. is supported by a NSERC grant.

Conflicts of Interest: The authors declare no conflict of interest.

References

1. Tao, J.X.; Wang, T.; Chen, Z.H.; Luo, Z.Z.; Xu, L.Q.; Hao, X.Y.; Cui, L.W. The Re–Os isotopic dating of molybdenite from the Wulandele molybdenum-copper polymetallic deposit in Sonid Zuoqi of Inner Mongolia and its geological significance. *Rock Miner. Anal.* **2009**, *28*, 249–253, (In Chinese with English Abstract).
2. Liu, Y.F.; Nie, F.J.; Jiang, S.H.; Hou, W.R.; Liang, Q.L.; Zhang, K.; Liu, Y. Geochronology of Zhunsujihua molybdenum deposit in Sonid Left Banner, Inner Mongolia, and its geological significance. *Miner. Depos.* **2012**, *31*, 119–128, (In Chinese with English Abstract).
3. Shang, H.S.; Gao, W.Y.; Shi, C.; Yu, C.L.; Zuo, Y.S.; Wang, T. Relationship between characteristics of tungsten and molybdenum ore deposit in Wurinitu and early Cretaceous granite. *Earth Sci. J. China Univ. Geosci.* **2012**, *37*, 1259–1267, (In Chinese with English Abstract).
4. Zeng, Q.D.; Liu, J.M.; Qin, K.Z.; Fan, H.R.; Chu, S.X.; Wang, Y.B.; Zhou, L.L. Types, characteristics, and time–space distribution of molybdenum deposits in China. *Int. Geol. Rev.* **2013**, *55*, 1311–1358. [CrossRef]
5. Zhang, X.J.; Lentz, D.R.; Yao, C.L.; Liu, R.; Yang, Z.; Mei, Y.X.; Fan, X.W.; Huang, F.; Qin, Y.; Zhang, K.; et al. Geochronology, geochemistry, and Sr–Nd–Pb–Hf isotopes of the Zhunsujihua granitoid intrusions associated with the molybdenum deposit, northern Inner Mongolia, China: Implications for petrogenesis and tectonic setting. *Int. J. Earth Sci.* **2018**, *107*, 687–710. [CrossRef]
6. Tao, J.X.; Zhong, R.; Zhao, Y.M.; Zheng, B.J. Geological characteristics and ore-prospecting criteria of the Ulandler porphyry molybdenum deposit in Sonid Left Banner, Inner Mongolia. *Acta Geosci. Sin.* **2010**, *31*, 413–422, (In Chinese with English Abstract).
7. Tao, J.X.; Wang, T.; Chen, Z.H.; Tang, W.; Wang, R.F. SHRIMP zircon U-Pb age of the fine-grained monzonitic granite in the Wulandele molybdenum-copper polymetallic ore deposit of Inner Mongolia and its significance. *Geol. Bull. China* **2017**, *36*, 1525–1530, (In Chinese with English Abstract).
8. Zhang, F.F.; Wang, Y.H.; Liu, J.J.; Wang, J.C. Ore genesis and hydrothermal evolution of the Wulandele Mo deposit, Inner Mongolia, Northeast China: Evidence from geology, fluid inclusions, and H–O–S–Pb isotopes. *Ore Geol. Rev.* **2018**, *93*, 181–199. [CrossRef]
9. Ye, M.; Zhang, S.H.; Wu, F.Y. The classification of the Paleozoic tectonic units in the area crossed by Manzhouli-Suifenghe geosciences transect. *J. Chang. Univ. Earth Sci.* **1994**, *24*, 241–245, (In Chinese with English Abstract).
10. Wu, F.Y.; Zhao, G.C.; Sun, D.Y.; Wilde, S.A.; Yang, J.H. The Hulan Group: Its role in the evolution of the Central Asian Orogenic Belt of NE China. *J. Asian Earth Sci.* **2007**, *30*, 542–556. [CrossRef]
11. Wu, F.Y.; Sun, D.Y.; Ge, W.C.; Zhang, Y.B.; Grant, M.L.; Wilde, S.A.; Jahn, B.M. Geochronology of the Phanerozoic granitoids in northeastern China. *J. Asian Earth Sci.* **2011**, *41*, 1–30. [CrossRef]
12. Zhou, Z.H.; Mao, J.W.; Lyckberg, P. Geochronology and isotopic geochemistry of the A-type granites from the Huanggang Sn-Fe deposit, southern Great Hinggan Range, NE China: Implication for their origin and tectonic setting. *J. Asian Earth Sci.* **2012**, *49*, 272–286. [CrossRef]

13. Shu, Q.H.; Chang, Z.S.; Lai, Y.; Zhou, Y.T.; Sun, Y.; Yan, C. Regional metallogeny of Mo-bearing deposits in northeastern China, with new Re-Os dates of porphyry Mo deposits in the northern Xilamulun district. *Econ. Geol.* **2016**, *111*, 1783–1798. [CrossRef]
14. Jahn, B.M.; Wu, F.Y.; Chen, B. Massive granitoid generation in Central Asia: Nd isotope evidence and implication for continental growth in the Phanerozoic. *Episodes* **2000**, *23*, 82–92. [CrossRef]
15. Du, A.D.; Wu, S.Q.; Sun, D.Z.; Wang, S.X.; Qu, W.J.; Markey, R.; Stein, H.; Morgan, J.; Malinovskiy, D. Preparation and certification of Re–Os dating reference materials: Molybdenite HLP and JDC. *Geostand. Geoanalytical Res.* **2004**, *28*, 41–52. [CrossRef]
16. Smoliar, H.J.; Walker, R.J.; Morgan, J.W. Re-Os ages of group IIA, IIIA, IVA, and IVB iron meteorites. *Science* **1996**, *271*, 1099–1102. [CrossRef]
17. Watson, E.B.; Harrison, T.M. Zircon saturation revisited: Temperature and composition effects in a variety of crustal magma types. *Earth Planet Sci. Lett.* **1983**, *64*, 295–304. [CrossRef]
18. Middlemost, E.A.K. *Magmas and Magmatics Rocks*; Longman: London, UK, 1985; 266p.
19. Peccerillo, A.; Taylor, S.R. Geochemistry of Eocene calc-alkaline volcanic rocks from the Kastamonu area, Northern Turkey. *Contrib. Mineral. Petrol.* **1976**, *58*, 63–81. [CrossRef]
20. Maniar, D.P.; Piccoli, M.P. Tectonic discrimination of granitoids. *GSA Bull.* **1989**, *101*, 635–643. [CrossRef]
21. Sun, S.S.; McDonough, W.F. Chemical and isotopic systematics of oceanic basalts: Implications for mantle composition and processes. In *Magmatism in the Ocean Basins*; Saunders, A.D., Norry, M.J., Eds.; Geological Society, Special Publication: London, UK, 1989; pp. 313–345.
22. Boynton, W.V. Cosmochemistry of the rare earth elements: Meteorite studies. In *Rare Earth Element Geochemistry*; Henderson, P., Ed.; Elsevier: Amsterdam, The Netherlands, 1984; pp. 63–114.
23. Wu, F.Y.; Jahn, B.M.; Wilde, S.; Sun, D.Y. Phanerozoic crustal growth: U-Pb and Sr-Nd isotopic evidence from the granites in northeastern China. *Tectonophysics* **2000**, *328*, 89–113. [CrossRef]
24. Liu, R.; Yang, Z.; Xu, Q.D.; Zhang, X.J.; Yao, C.L. Zircon U-Pb ages, elemental and Sr-Nd isotopic geochemistry of the Hercynian granitoids from the southern segment of the Dahinggan Mts: Petrogenesis and tectonic implications. *Acta Petrol. Sin.* **2016**, *32*, 1505–1528, (In Chinese with English Abstract).
25. Lu, Y.F. GeoKit—A geochemical toolkit for Microsoft Excel. *Geochimica* **2004**, *33*, 459–464.
26. Whalen, J.B.; Currie, K.L.; Chappell, B.W. A-type granites: Geochemical characteristics, discrimination and petrogenesis. *Contrib. Mineral. Petrol.* **1987**, *95*, 407–419. [CrossRef]
27. Barbarin, B. Granitoids: Main petrogenetic classifications in relation to origin and tectonic setting. *Geol. J.* **1990**, *25*, 227–238. [CrossRef]
28. Barbarin, B. A review of the relationships between granitoid types, their origins and their geodynamic environments. *Lithos* **1999**, *46*, 605–626. [CrossRef]
29. Zartman, R.E.; Doe, B.R. Plumbotectonics—The model. *Tectonophysics* **1981**, *75*, 135–162. [CrossRef]
30. Pearce, J.A. Sources and settings of granitic rocks. *Episodes* **1996**, *19*, 120–125. [CrossRef]
31. Christiansen, E.H.; Keith, J.D. Trace element systematics in silicic magmas: A metallogenic perspective. In *Trace Element Geochemistry of Volcanic Rocks: Applications for Massive Sulphide Exploration*; Short Course Notes; Wyman, D., Ed.; Geological Association of Canada: St. John's, NL, Canada, 1996; Volume 12, p. 115.
32. Harris, N.B.W.; Pearce, J.A.; Tindle, A.G. Geochemical characteristics of collision zone magmatism. In *Collision Tectonics*; Geol. Soc. Spec. Publ. London; Coward, M.P., Ries, A.C., Eds.; Geological Society: Leicester, UK, 1986; Volume 19, pp. 67–81.
33. Batchelor, R.A.; Bowden, P. Petrogenetic interpretation of granitoid rock series using multicationic parameters. *Chem. Geol.* **1985**, *48*, 43–55. [CrossRef]
34. Zonenshain, L.P.; Kuzmin, M.I.; Natapov, L.M. *Geology of USSR: A Plate-Tectonic Synthesis*; Geodynamics Series; American Geophysical Union: Washington, DC, USA, 1990; Volume 21, 242p.
35. Enkin, R.J.; Yang, Z.; Chen, Y.; Courtillot, V. Paleomagnetic constraints on the geodynamic history of the major blocks of China from the Permian to the present. *J. Geophys. Res. Solid Earth* **1992**, *97*, 13953–13989. [CrossRef]
36. Sengör, A.M.C.; Natal'in, B.A. Paleotectonics of Asia: Fragments of a synthesis. In *The Tectonic Evolution of Asia*; Yin, A., Harrison, T.M., Eds.; Cambridge University Press: Cambridge, UK, 1996; pp. 486–641.
37. Scotese, C.R. *Atlas of Earth History*; PALEOMAP Project: Arlington, TX, USA, 2001; p. 58.

38. Kravchinsky, V.A.; Cogné, J.P.; Harbert, W.P.; Kuzmin, M.I. Evolution of the Mongol–Okhotsk Ocean as constrained by new palaeomagnetic data from the Mongol–Okhotsk suture zone, Siberia. *Geophys. J. Int.* **2002**, *148*, 34–57. [CrossRef]
39. Tomurtogoo, O.; Windley, B.F.; Kröner, A.; Badarch, G.; Liu, D.Y. Zircon age and occurrence of the Adaatsag ophiolite and Muron shear zone, central Mongolia: Constraints on the evolution of the Mongol-Okhotsk ocean, suture and orogen. *J. Geol. Soc.* **2005**, *162*, 125–134. [CrossRef]
40. Chen, Y.J.; Zhang, C.; Wang, P.; Pirajno, F.; Li, N. The Mo deposits of northeast China: A powerful indicator of tectonic settings and associated evolutionary trends. *Ore Geol. Rev.* **2017**, *81*, 602–640. [CrossRef]
41. Wang, P.; Chen, Y.J.; Wang, C.M.; Wang, S.X. Genesis and tectonic setting of the giant Diyanqinamu porphyry Mo deposit in Great Hingan Range, NE China: Constraints from U–Pb and Re–Os geochronology and Hf isotopic geochemistry. *Ore Geol. Rev.* **2017**, *81*, 760–779. [CrossRef]
42. Keith, J.D.; Christiansen, E.H.; Carten, R.B. The genesis of giant porphyry molybdenum deposits. In *Giant Ore Deposits*; Whiting, B.H., Mason, R., Hodgson, C.J., Eds.; Society of Economic Geologists Special Publication: London, UK, 1993; Volume 2, pp. 285–316.
43. Tacker, R.C.; Candela, P.A. Partitioning of molybdenum between magnetite and melt: A preliminary experimental study of partitioning of ore metals between silicic magmas and crystalline phases. *Econ. Geol.* **1987**, *82*, 1827–1838. [CrossRef]
44. Blevin, P.L. Redox and compositional parameters for interpreting the granitoid metallogeny of eastern Australia: Implications for gold-rich ore systems. *Resour. Geol.* **2004**, *54*, 241–252. [CrossRef]
45. Ishihara, S. *The Granitiod Series and Mineralization*; Economic Geology 75th Anniversary Volume 1981; Economic Geology Publishing Company: Littleton, CO, USA, 1981; pp. 458–484.
46. Govett, G.J.S.; Atherden, P.R. Applications of rock geochemistry to productive plutons and volcanic sequences. *J. Geochem. Explor.* **1988**, *30*, 223–242. [CrossRef]
47. Meinert, L.D. Compositional variation of igneous rocks associated with skarn deposits-chemical evidence for a genetic connection between petrogenesis and mineralization. In *Magmas, Fluids, and Ore Deposits*; Min. Assoc. Can. Short Course Series; Thompson, J.F.H., Ed.; Mineralogical Association of Canada: Quebec, QC, Canada, 1995; Volume 23, pp. 401–418.
48. Candela, P.A.; Holland, H.D. A mass transfer model for copper and molybdenum in magmatic hydrothermal systems: The origin of porphyry-type ore deposits. *Econ. Geol.* **1986**, *81*, 1–19. [CrossRef]
49. El Bouseily, A.M.; El Sokkary, A.A. The relation between Rb, Ba and Sr in granitic rocks. *Chem. Geol.* **1975**, *16*, 207–219. [CrossRef]
50. Liu, J.T.; Yang, L.Q.; Lü, L. Pulang reduced porphyry copper deposit in the Zhongdian area, Southwest China: Constrains by the mineral assemblages and the ore-forming fluid compositions. *Acta Petrol. Sin.* **2013**, *29*, 3914–3924.
51. Zeng, Q.D.; Chu, S.X.; Wang, Y.B.; Liu, J.M.; Sun, Y.; Duan, X.X.; Zhou, L.L.; Qu, W.J. Re–Os and U–Pb geochronology of the Duobaoshan porphyry Cu–Mo–(Au) deposit, northeast China, and its geological significance. *J. Asian Earth Sci.* **2014**, *79*, 895–909. [CrossRef]
52. Qin, K.Z.; Li, H.M.; Li, W.S.; Shunso, I. Intrusion and mineralization ages of the Wunugetushan porphyry Cu–Mo deposit, Inner Mongolia, northwestern China. *Geol. Rev.* **1999**, *45*, 180–185, (In Chinese with English Abstract).
53. Jacobsen, S.B.; Wasserburg, G.J. Sm–Nd isotopic evolution of chondrites. *Earth Planet. Sci. Lett.* **1980**, *50*, 139–155. [CrossRef]